Available online at www.sciencedirect.com
ScienceDirect
Thermochimica Acta 448 (2006) 73–81
thermochimica acta
www.elsevier.com/locate/tca

Observation of multiple phase transitions in some even *n*-alkanes using a high resolution and super-sensitive DSC

Shaolan Wang [a,*], Ken-Ichi Tozaki [b], Hideko Hayashi [b], Hideaki Inaba [b], Hiroko Yamamoto [c]

[a] *Graduate School of Science and Technology, Chiba University, 1-33 Yayoi-Chou, Inage-ku, Chiba 263-8522, Japan*
[b] *Faculty of Education, Chiba University, 1-33 Yayoi-Chou, Inage-ku, Chiba 263-8522, Japan*
[c] *Department of Molecular and Material Sciences, IGSES, Kyushu University, 6-1 Kasuga-koen, Kasuga, Fukuoka 816-8580, Japan*

Received 14 October 2005; received in revised form 28 June 2006; accepted 28 June 2006
Available online 4 July 2006

Abstract

The phase transitions of even *n*-alkanes, *n*-$C_{34}H_{70}$, *n*-$C_{36}H_{74}$, *n*-$C_{40}H_{82}$ and *n*-$C_{42}H_{86}$ with high purity have been measured using a high resolution and super-sensitive DSC. A new transition in the low temperature phase was observed in all the samples in the heating run. The surface freezing phenomenon was observed by thermal measurement for the first time in all the samples both in the heating and in the cooling run. The difference of the thermal behaviors between the heating and cooling run was also observed in all the samples.

Keywords: DSC; *n*-Alkane; Phase transition; Surface freezing; Rotator phase

1. Introduction

The normal alkanes C_nH_{2n+2} are simple organic systems and sequences of C_nH_{2n} can be found in lipids, surfactants, liquid crystals, and polymers. The stable phases of the *n*-alkanes at room temperature assume different crystal structures due to the differences in molecular chain symmetry of the molecules with even or odd carbon numbers. The crystals of even numbered *n*-alkane molecules ($n \geq 26$) are monoclinic with the plane of the methyl-ends tilted to the molecular chain axis [1,2]. On the other hand, the crystals of the odd numbered *n*-alkanes with a perpendicular symmetry plane for the molecular chain axis are orthorhombic [3]. The solid–solid transitions have been observed in the normal alkanes by various methods [4–11]. The structural change of these transitions seems to be effected by both the sample purity and the crystallization conditions [12,13]. When crystallized from a solution, even *n*-alkanes sometime assume the monoclinic form and in other case the orthorhombic form. Impurities generally lead to the orthorhombic form, and the shorter even *n*-alkanes always crystallized in the monoclinic form, which is the most stable phase at room temperature for even *n*-paraffins and denoted by M_{011} according to the Sullivan–Weeks' notation [12]. M_{011} form is achieved mostly by crystallization at a very slow cooling rate from solution [13]. Another monoclinic form is observed at higher temperature and denoted by M_{h01} (usually $h = 1$ or 2) [13]. The characteristics of *n*-alkanes have been studied by various methods, but only a few measurements have been done during the cooling process [14,15] and only a few have been reported for the normal alkanes with $n \geq 40$, especially for even *n*-alkanes [12,13].

n-Alkanes with $9 \leq n$ (odd) ≤ 39 and with $20 \leq n$ (even) ≤ 38 have characteristic crystalline phases, which are commonly called rotator phases (R phases), just below their melting points [16–19]. In these phases, the molecules undergo a segmental rotation and which as a time-average yields a cylindrical symmetry for the whole molecule. Sirota et al. [20] found five R phases for C_nH_{2n+2} with $20 \leq n \leq 33$, which are characterized in terms of the molecular tilt, side packing, azimuthal ordering and layer stacking by X-ray scattering study. They [21] also made a calorimetric study of the *n*-alkanes: C_nH_{2n+2} ($20 \leq n \leq 30$) using an adiabatic scanning calorimeter and found the phase transitions corresponding to the rotator phases detected by the X-ray scattering study [20]. However, their measurement was limited up to $C_{30}H_{62}$ for the *n*-alkanes.

Wu et al. [22,23] discovered the surface freezing phenomenon, in which a thin layer at an air/liquid interface crystal-

* Corresponding author. Tel.: +81 43 290 2599; fax: +81 43 290 2519.
E-mail address: aihongye@office.chiba-u.jp (S. Wang).

0040-6031/$ – see front matter © 2006 Elsevier B.V. All rights reserved.
doi:10.1016/j.tca.2006.06.022

lizes during cooling at about 3 K higher than the bulk melting point in molten normal alkanes C_nH_{2n+2} ($16 \leq n \leq 50$) using X-ray and surface tension measurements. Yamamoto and co-workers [24–26] investigated this phenomenon using the molecular simulation method. Magonov and co-workers [27] found the surface freezing even on solid surfaces on long-chain alkanes. We detected the surface freezing phenomenon on the liquid surface of n-$C_{22}H_{46}$ for the first time by the thermal measurement [28].

Thermal measurement is a powerful tool to obtain thermodynamic information for the phase transitions of n-alkanes [29–33]. We have developed a high resolution and super-sensitive DSC [34] capable of measuring a small heat with a small baseline fluctuation and a small drift of the baseline and a quick response time at a slow heating rate using small amount of sample. It is also capable of measuring in the both direction of heating and cooling, since some sorts of materials in the cooling process often show a different behavior from the heating process [28,35,36].

In the present paper, the phase transitions of n-$C_{34}H_{70}$, n-$C_{36}H_{74}$, n-$C_{40}H_{82}$ and n-$C_{42}H_{86}$ with high purity have been measured at slow heating and cooling rates using the high resolution and super-sensitive DSC. The detailed behaviors of the new solid–solid transitions, the different behaviors of the transitions between the heating and the cooling run and the surface freezing phenomenon have been shown and their mechanisms have been discussed.

2. Experimental

2.1. Apparatus

We have used a high resolution and super-sensitive heat-flux type differential scanning calorimeter (DSC), which was described previously [34]. The schematic drawing of the DSC is shown in Fig. 1. Since the thermoelectric module, TM5 can pump heat in either direction to heat or cool the copper blocks by changing the direction of the current through it, the measurement can be made in either direction of heating or cooling with this apparatus. The temperature region measurable in the DSC is between 220 and 400 K. The temperature of the sample was measured using a Pt resistance thermometer, TS1. The calibration of temperature of TS1 was made by measuring the melting point of the standard materials, such as docosane, biphenyl, Ga and H_2O. The calibration of heat flow was made by measuring the specific heat capacity of the standard sample of a single crystalline alumina. The specific heat capacity of alumina was measured within an inaccuracy of 1%. The temperature control was made within ±0.15 mK and the stability of the baseline was within ±3 nW at 300 K.

2.2. Sample

We used n-alkanes of n-$C_{34}H_{70}$, n-$C_{36}H_{74}$, n-$C_{40}H_{82}$ and n-$C_{42}H_{86}$ with high purity in present measurements because it is known that the phase transitions of n-alkanes are apt to be affected by homologous impurities [12]. They were synthesized

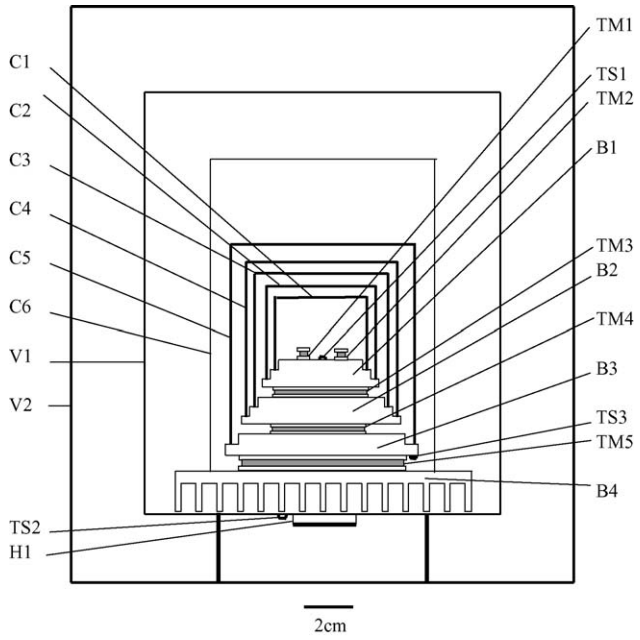

Fig. 1. Schematic drawing of the high resolution and super-sensitive DSC [34], where TS1–3 are Pt resistance thermometers, C1–6 are copper shields, B1–3 are copper blocks, B4 is an aluminum block, TM1 and TM2 are semiconducting temperature sensors, TM3–5 are semiconducting thermoelectric modules, H1 is heater, V1 is enclosing metal vessel and V2 is refrigerating vessel.

by using Wurtz condensation method and their purity was higher than 99.9% determined by gas chromatography (Shimazu GC-14A). All the samples are the same as that already reported by Takamizawa group of Kyushu University [13,37]. The sample was enclosed in an aluminum capsule with air for the DSC measurement. The sample amount was 0.65, 0.65, 0.41 and 0.71 mg for n-$C_{34}H_{70}$, n-$C_{36}H_{74}$, n-$C_{40}H_{82}$ and n-$C_{42}H_{86}$, respectively. The measurements were made in air and the reference was an empty Al pan. The temperature range is from 313.15 to 353.15 K for $C_{34}H_{70}$ and from 323.15 to 363.15 K for other samples. In every measurement the samples were kept at the temperature of 10 K above their melting point for an hour before cooling. We made these measurements several times and found that the curves were almost the same. The data shown in these figures were those of the third or the fourth one.

3. Results

The DSC measurements were made at the heating rate of 1 mK s^{-1} and at the cooling rate of 0.5 mK s^{-1} for all the samples. The DSC curves for $C_{34}H_{70}$, $C_{36}H_{74}$, $C_{40}H_{82}$ and $C_{42}H_{86}$ are shown in Figs. 2(a), 3(a), 4(a) and 5(a), respectively. The heating results are shown downwards and the cooling results are shown upwards in these figures. The magnified curves of them are shown in Figs. 2(b), 3(b), 4(b) and 5(b), respectively. In the magnified curves, the first peak at the highest temperature is named peak 1 in the heating run and that in the cooling run is named peak 1′. Similarly, the second, third and fourth peak are named peak 2, peak 3, and peak 4, respectively for the heating run, and there are named peak 2′, peak 3′, and peak 4′, respectively for the cooling run. The Arabic numerals are the

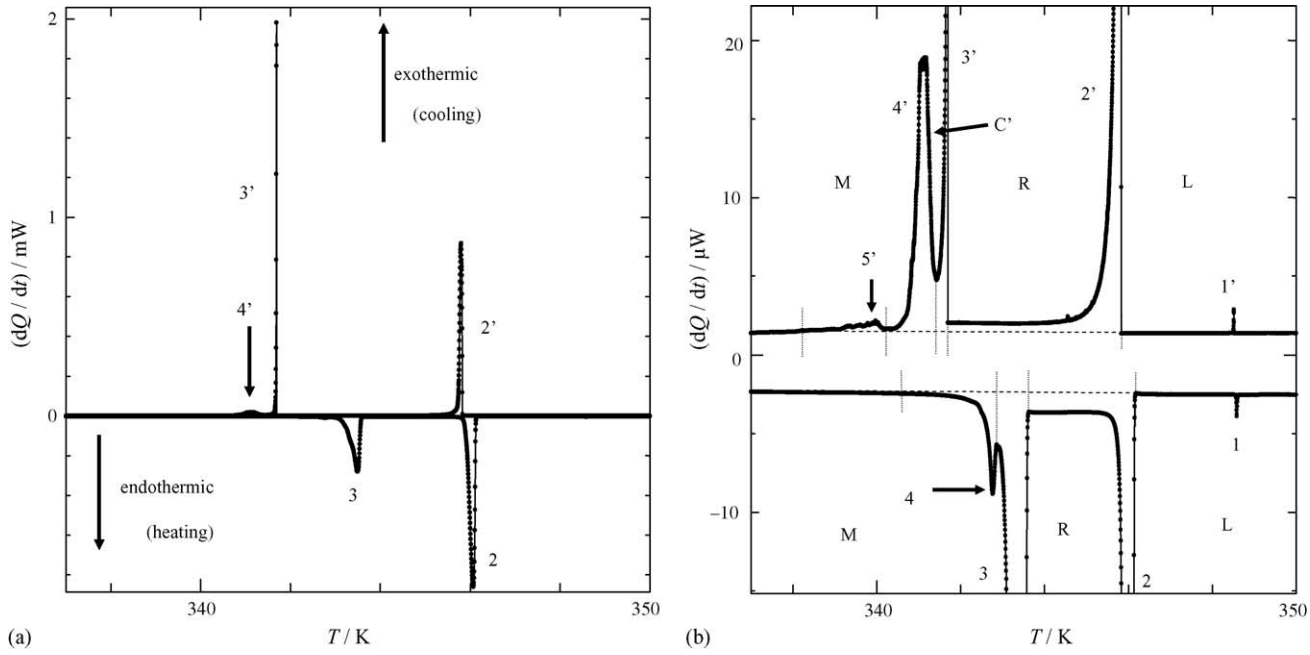

Fig. 2. DSC curve of $C_{34}H_{70}$ sample at the heating rate of 1 mK s^{-1} and the cooling rate of 0.5 mK s^{-1}; (a) full scale drawing and (b) magnified scale.

peaks number of the DSC curves and the Roman letters mean the phase of the samples (L means liquid phase, R means rotator phase, etc.).

The transition temperatures were obtained from the peak temperatures and listed in Tables 1 and 2.

The peak 2 in all of these curves are due to melting [16,37], and the peak 2′ are due to solidification. The melting points of $C_{34}H_{70}$, $C_{36}H_{74}$, $C_{40}H_{82}$ and $C_{42}H_{86}$ are obtained as 346.1, 349.2, 354.6 and 357.3 K, respectively, they are in good agreement with the results by Kraack et al. [14], Briard et al. [15], Broadhurst [16], Urabe et al. [37] and Kim et al. [38].

Peak 1 in all of these curves was observed about 2 K above the melting temperature as shown in Figs. 2(b), 3(b), 4(b) and 5(b). It is considered to be due to the surface freezing phenomenon [22]. The corresponding peak in the cooling run (peak 1′) was also observed at nearly the same temperature for each run. The thermal peak due to the surface freezing phenomenon using a bulk sample is detected for the first time in these samples, showing the high sensitivity of the present DSC.

The baseline drawn from the M phase to the liquid phase for calculating the enthalpy of the transitions was shown in the figures with a dash line. The area of each peak was discriminated

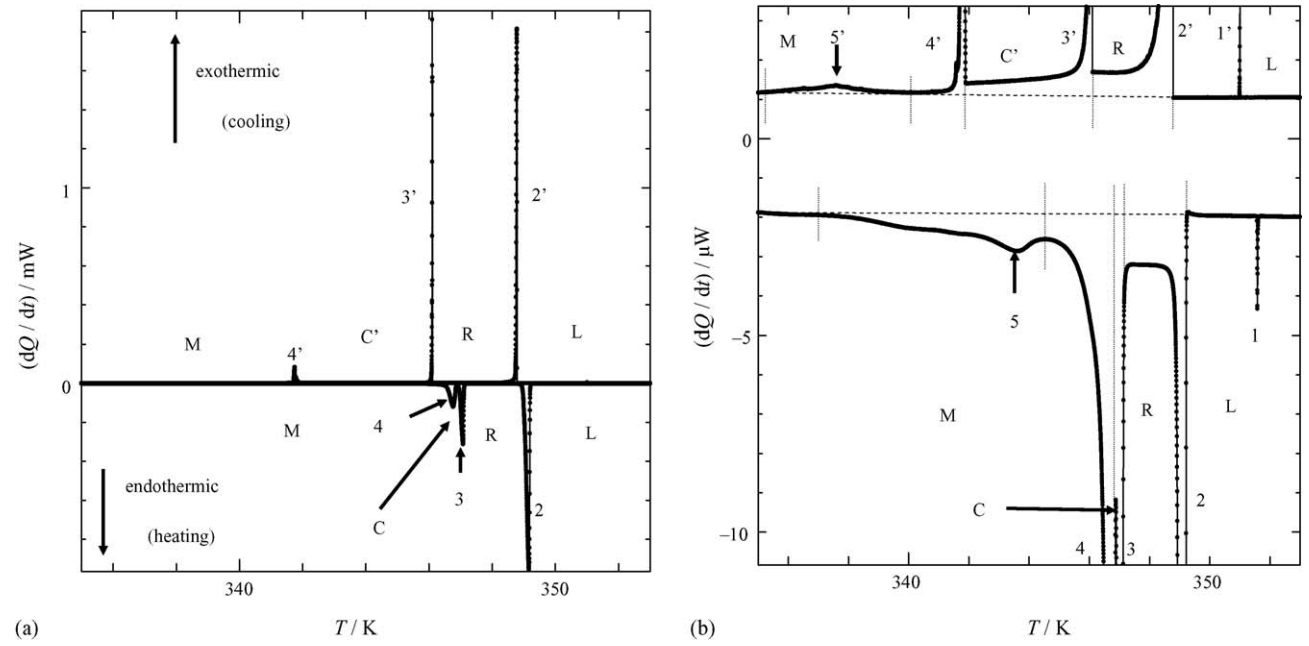

Fig. 3. DSC curve of $C_{36}H_{74}$ sample at the heating rate of 1 mK s^{-1} and the cooling rate of 0.5 mK s^{-1}; (a) full scale drawing and (b) magnified scale.

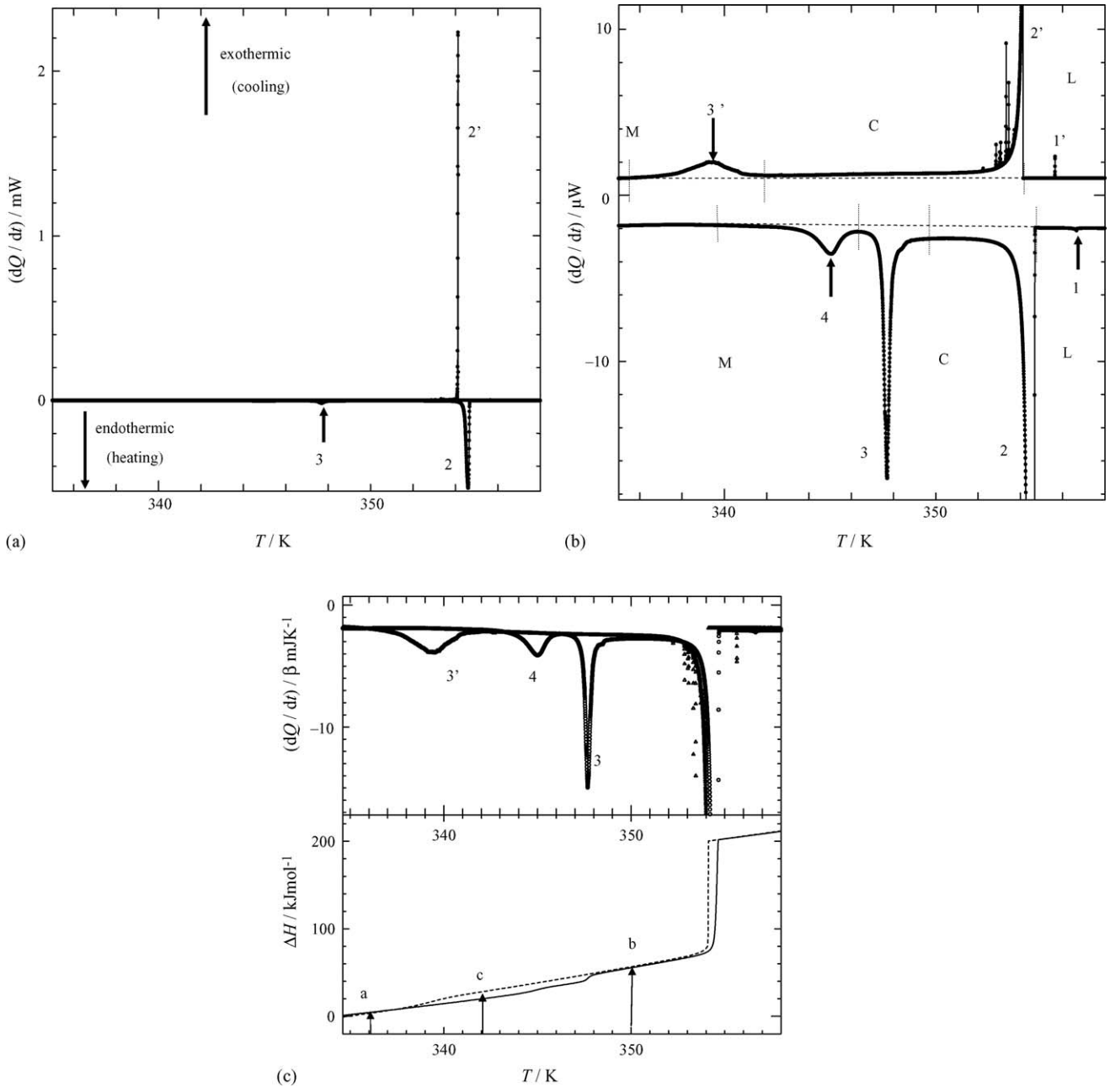

Fig. 4. DSC curve of $C_{40}H_{82}$ sample at the heating rate of 1 mK s^{-1} and the cooling rate of 0.5 mK s^{-1}; (a) full scale drawing, (b) magnified scale, and (c) the relative enthalpy of the whole process of the heating and cooling run together with the DSC curves, where (◯) and solid line correspond to the heating run; (△) and the dotted line correspond to the cooling run. In order to compare the DSC curves of the heating and the cooling run, the value of the vertical axis is divided by the heating/cooling rate (β) and the direction of the DSC curve of cooling run was reversed.

with the dotted line, drawing from the nearest point of the DSC curves and perpendicular to the baseline. The enthalpy changes of the peaks are obtained by integrating the area of them and listed in Tables 1 and 2.

3.1. $C_{34}H_{70}$

The DSC curves for $C_{34}H_{70}$ are shown in Fig. 2(a) and the magnified curves of them are shown in Fig. 2(b). Peak 3 centered at 343.5 K is known as due to the solid–solid transition from the low-temperature phase (M phase) to the rotator phase [16,37]. The structure of M phase is considered to be M_{011} [13,37]. The temperature of peak 3 is in good agreement with the result obtained by Gilbert [39], 343.15 K. Peak 4 was observed at 342.8 K in Fig. 2(b), just below the temperature of peak 3 in the heating run.

Peak 3′ is due to the solid–solid transition from the rotator phase to the M phase. Peak 4′ is the new peak detected in cooling run. Another small peak (peak 5′) was observed at the low temperature side of peak 4′. From the fact that the sum of enthalpy change of peaks 3′ and 4′ in the cooling run and that of peak 3 in the heating run are almost the same as shown in

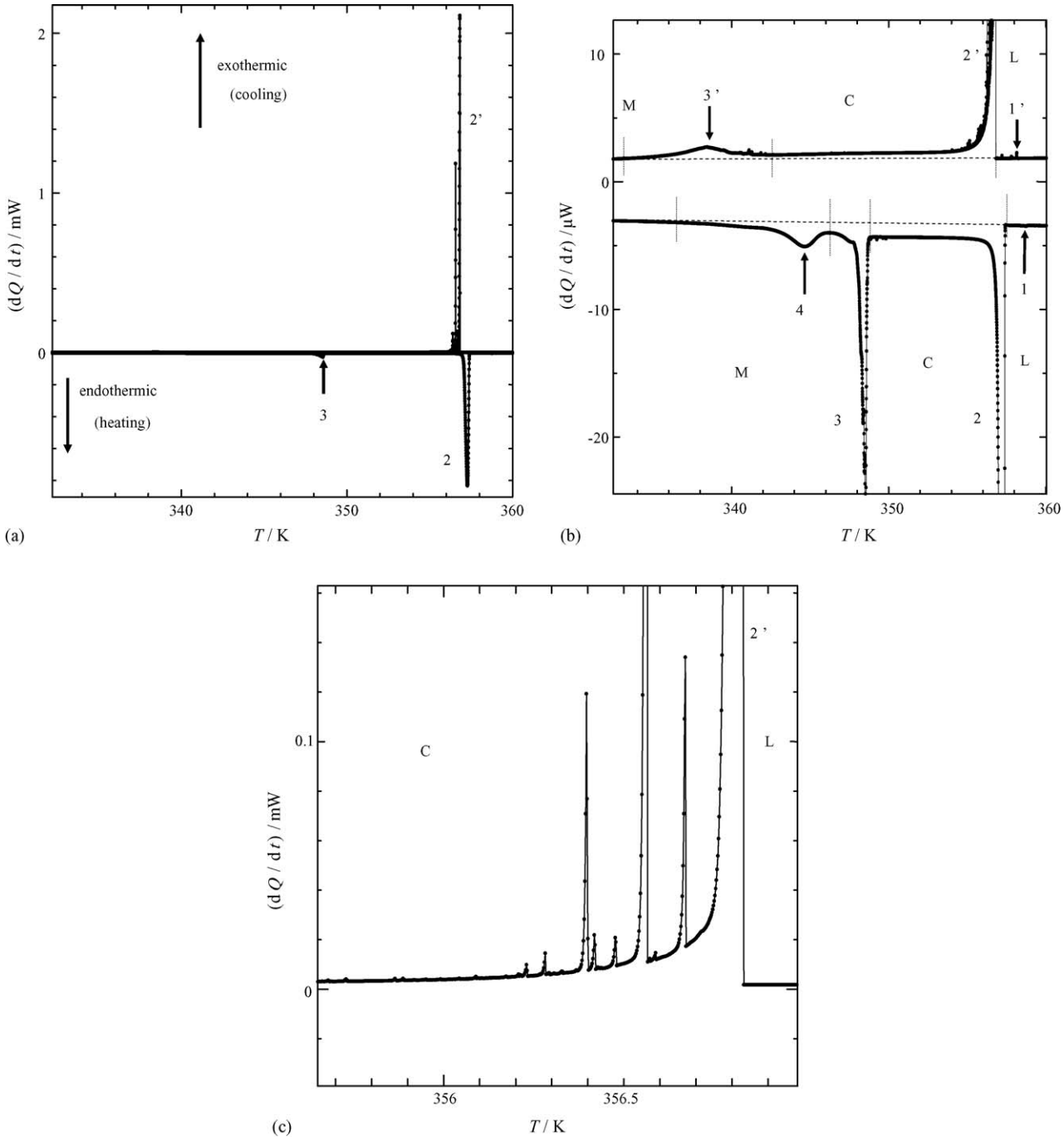

Fig. 5. DSC curve of $C_{42}H_{86}$ sample at the heating rate of 1 mK s^{-1} and the cooling rate of 0.5 mK s^{-1}; (a) full scale drawing, (b) magnified scale, and (c) magnified scale around melting point in the cooling run.

Table 1, peak 3 in the heating run is considered to be separated into peaks 3′ and 4′ in the cooling run, showing the appearance of a new phase between the R phase and the M phase. The structure of the new phase is still uncertain, but considered to be C phase. This phase is observed in even number *n*-alkane ($n \geq 36$) [4,16]. However, Takamizawa et al. [13] insisted the existence of C phase might be extended to *n*-$C_{32}H_{66}$, even if the DSC peak cannot be resolved. Because it cannot be observed in the heating run, C phase in the cooling run of $C_{34}H_{70}$ is considered to be metastable and named as C′ phase in the present paper. Peak 5′ in the cooling run is considered to correspond with the peak 4 in the heating run, because the enthalpy change of peak 4 are almost equal to that of peak 5′ as shown in Table 1. Since the enthalpy changes are very small, the origin of peak 4 and peak 5′ are considered to be related to the thermal behavior of the molecular chain ends in the low-temperature phase [35]. As seen in Fig. 2(b), the baseline of the heat flux in the rotator phase is about 2 μW higher than that in the M phase both in the heating and in the cooling run, which indicates that the heat capacity of the rotator phase is higher than that of the M phase, resulting from the rotational action of the molecular chains.

Table 1
The temperatures and enthalpy changes of the phase transitions in $C_{34}H_{70}$ and $C_{36}H_{74}$

Transitions	Surface freezing	L ⇔ R	R ⇔ M		New transition in M phase
$C_{34}H_{70}$					
Heating					
Peak number	1	2	3		4
T (K)	348.6	346.1	343.5		342.8
ΔH (kJ mol^{-1})	0.022	95.638	46.654		0.405
Cooling					
Peak number	1′	2′	3′	4′	5′
T (K)	348.5	345.8	341.7	341.1	339.9
ΔH (kJ mol^{-1})	0.023	99.212	35.882	8.135	0.381
Transitions	Surface freezing	L ⇔ R	R ⇔ C	C ⇔ M	New transition in M phase
$C_{36}H_{74}$					
Heating					
Peak number	1	2	3	4	5
T (K)	351.6	349.2	347.1	346.8	343.6
ΔH (kJ mol^{-1})	0.029	102.510	28.523	15.017	0.467
Cooling					
Peak number	1′	2′	3′	4′	5′
T (K)	351.0	348.8	346.1	341.8	337.6
ΔH (kJ mol^{-1})	0.029	106.322	33.008	6.745	0.780

3.2. $C_{36}H_{74}$

The DSC curves for $C_{36}H_{74}$ are shown in Fig. 3(a) and the magnified curves of them are shown in Fig. 3(b). We can see three large endothermic peaks centered at 346.8 K (peak 4), 347.1 K (peak 3) and 349.2 K (peak 2) in the heating run from Fig. 3(a), which are different with the heating run of $C_{34}H_{70}$ shown in Fig. 2(a). The reason is considered to be the observation of C phase in the heating run. Takamizawa et al. [13] confirmed the structure of C phase to be M_{101} by X-ray scattering and optical microscopy. In this phase, the *n*-alkane crystals are still monoclinic with the plane of the methyl-ends tilted to the molecular chain axis, but the angle is sharper compared to the M phase [12]. The C phase is described as an intermediate form between the crystalline phase and the liquid phase, which exists in a very narrow temperature for $C_{36}H_{74}$ [4]. Peak 4 is known as due to the solid–solid transition from the M phase to the C phase and peak 3 is known as due to the solid–solid transition from the C phase to the rotator phase [16,37]. The temperature of peak 3 is in good agreement with the result of Broadhurst [16], 347.0 K. Peak 5 was observed around 343.6 K in the heating run from Fig. 3(b). It is considered to be the new peak detected in the M phase of $C_{36}H_{74}$, corresponding to the peak 4 of $C_{34}H_{70}$ shown in Fig. 2(b).

Peak 3′ and peak 4′ in the cooling run are considered to correspond with the peak 3 and peak 4, respectively. From the enthalpy changes of the peaks shown in Table 1, we can see the enthalpy change of peak 3′ is larger than that of peak 3, and the enthalpy change of peak 4′ is smaller than that of peak 4, although the sum of them in the heating run almost equals to that of the cooling run. Although the transition between the M phase and the rotator phase is the same in the heating and the cooling run, the intermediate form appeared in the cooling run is probably different with that of heating run (C phase). It is named as C′ phase in the present paper. Therefore, peak 3′ is due to the solid–solid transition from the rotator phase to the C′ phase and peak 4′ is due to the solid–solid transition from the C′ phase to the M phase. The vibrational motion of the molecule in the C phase and C′ phase

Table 2
The temperatures and enthalpy changes of the phase transitions in $C_{40}H_{82}$ and $C_{42}H_{86}$, the values in the parenthesis are those be obtained from the relative enthalpy as shown in Fig. 4(c)

Transitions	Surface freezing	L ⇔ C	C ⇔ M	New transition in M phase
$C_{40}H_{82}$				
Heating				
Peak number	1	2	3	4
T (K)	356.7	354.6	347.7	345.0
ΔH (kJ mol^{-1})	0.024	143.941 (152.427)	8.596 (16.487)	2.513 (25.629)
Cooling				
Peak number	1′	2′	3′	
T (K)	355.7	354.1	339.5	
ΔH (kJ mol^{-1})	0.024	147.102 (150.707)	6.350(44.751)	
$C_{42}H_{86}$				
Heating				
Peak number	1	2	3	4
T (K)	358.8	357.3	348.6	344.6
ΔH (kJ mol^{-1})	0.007	165.967 (174.828)	8.457 (16.376)	2.110 (24.574)
Cooling				
Peak number	1′	2′	3′	
T (K)	358.2	356.8	338.5	
ΔH (kJ mol^{-1})	0.008	170.318 (174.013)	5.982(42.071)	

is considered to change with the temperature significantly and continuously, being the same phenomenon observed in $C_{51}H_{104}$ [40]. It causes the much larger heat capacity of C phase and C′ phase than that of the liquid. A small peak (peak 5′) is observed in the cooling run in Fig. 3(b). It is considered to be the new peak corresponding to the peak 5 in the heating run.

3.3. $C_{40}H_{82}$ and $C_{42}H_{86}$

The DSC curves for $C_{40}H_{82}$ and $C_{42}H_{86}$ are shown in Figs. 4(a) and 5(a), respectively. The magnified curves are shown in Figs. 4(b) and 5(b), respectively. From these curves and the enthalpy changes of the peaks shown in Table 2, we can see the thermal behavior of the $C_{42}H_{86}$ is similar to that of $C_{40}H_{82}$. The mechanism of these phase transitions is considered to be the same.

Peaks 3 centered at 347.7 K in the Fig. 4(b) and 348.6 K in Fig. 5(b) are due to the solid–solid transition from the M phase to the C phase. Peaks 4 observed around 345.0 K in Fig. 4(b) and 344.6 K in Fig. 5(b) are the new peak detected in the M phase in $C_{40}H_{82}$ and $C_{42}H_{86}$, which correspond with the peak 4 of $C_{34}H_{70}$ in Fig. 2(b) and the peak 5 of $C_{36}H_{74}$ in Fig. 3(b). The rotator phase was not observed in both $C_{40}H_{82}$ and $C_{42}H_{86}$, in agreement with the result that the rotator phase is only observed in the *n*-alkanes with $9 \leq n$ (odd) ≤ 39 and with $20 \leq n$ (even) ≤ 38 [16].

The measurements of reheating the $C_{40}H_{82}$ sample after cooling from the liquid to the temperature of 342 or 335 K have been done. In the case of 342 K, neither peak 3 nor peak 4 could observed in the heating run, On the other hand, both of peak 3 and peak 4 were observed in the case of 335 K. The results show that peak 3′ in the cooling run is due to the solid–solid transition from C phase to M phase. In the heating run, the transition from M phase to C phase separates into two steps via a mesophase as seen in the peaks 3 and 4 in Figs. 4(b) and 5(b). In the cooling run, it changes directly from C phase to M phase as seen in the peak 3′ in Figs. 4(b) and 5(b). Therefore the new phase was not observed in the cooling run. The enthalpy changes obtained by integrating the area of the peaks in Figs. 4(b) and 5(b) and are shown in Table 2. In Table 2, the enthalpy change of peak 3′ was not equal to the total of peaks 3 and 4. In order to explain the peak 3′ clearly, the relative enthalpy of the whole process of the heating and cooling run for $C_{40}H_{82}$ was shown in Fig. 4(c) together with the DSC curves. In Fig. 4(c), the sample state at 336 and 350 K and that in the cooling run at 342 K is named state a, b and c, respectively. It is known from Fig. 4(c) that both in the state a and in the state b, the relative enthalpy in the heating run is nearly equal to that of the cooling run. The values shown in the parenthesis in Table 2 are those obtained from the figure of relative enthalpy as Fig. 4(c). From those values, it is clear that the enthalpy change of peak 3′ was nearly equal to the total of peaks 3 and 4. It is clear from Fig. 4(c) that the C phase in the cooling run extends over a wide temperature range and the heat capacity of C phase is large. Then the enthalpy change between a and b is about two times of that between a and c (the transition from C phase to M phase) in the cooling run.

Many very sharp anomalies are also observed around 353.2 K in Fig. 4(b) and around 356.5 K in Fig. 5(a) in addition to the transition from the liquid phase to the C phase. This phenomenon was also observed in the case of $C_{22}H_{46}$ [28] and $C_{32}H_{66}$ [35]. The magnified curve of these peaks in Fig. 5(a) is shown in Fig. 5(c), where the peaks are observed more clearly. Around the temperature of 356.5 K in the cooling run of $C_{42}H_{86}$, the main solidification process is already accomplished and the liquid phase is considered to remain only in grain-boundary regions of each grain. During the very slow cooling process, the C phase grains intergrow by absorbing other grains, resulting in the exothermic peaks due to the more ordered grain-boundary regions.

4. Discussion

The surface freezing phenomenon was observed in all the samples both in the heating and in the cooling run as shown in peaks 1 and 1′ in Figs. 2(b), 3(b), 4(b) and 5(b). Such small thermal peaks were detected for the first time in these samples, showing the high sensitivity of the present DSC. The peaks 1′ in the cooling run are sharper than peaks 1 in the respective heating run in these figures, but the enthalpy change of peak 1′ is almost the same as that of peak 1 for each sample. The fact that the observed enthalpy changes in present paper are about several times larger than the calculated one indicates that the ordered phase on the surface of liquid alkane could be two or three molecular layers. Therefore the term “surface layer” is used instead of “monolayer” in this paper. The temperature difference between the melting of the bulk sample (T_m) and the fusion of the surface layer (T_f) decreases with the carbon number *n*, in our measurement. The temperature difference $\Delta T(=T_f - T_m)$ in the heating run are plotted against the carbon number *n* as shown in Fig. 6, where the literature data [22] obtained by X-ray and surface tension measurements are also shown for comparison. The present results are in good agreement with the literature data.

The phase transitions in the heating run for $C_{34}H_{70}$, $C_{36}H_{74}$, $C_{40}H_{82}$ and $C_{42}H_{86}$ obtained by the present measurements are summarized in Fig. 7, where the fusion of the surface layer is shown as the full square symbol with the dotted line. The new transition is shown with full circle symbol in Fig. 7. Since the new transition is observed in the M phase, the mesophase is named M′ phase in the present paper.

The transition observed in the M phase of these samples is the new transition detected by the present DSC. Kitamaru et al. [11], Jarrett et al. [31] and Ishikawa et al. [41] studied the molecular motion of *n*-alkanes by using ^{13}C NMR spectrometry and found that the molecular motion of CH_3, α-CH_2, β-CH_2 and γ-CH_2 were different from that of the internal-CH_2. Some fluctuational motion around the C–C bond occurs in the vicinity of the molecular ends, even below the temperature of the rotator transition [11]. Kim et al. [38] reported the fractional change of gauche bonds of alkanes per chain as a function of temperature from infrared spectra. They disordered gauche bonds become significant as the temperature increases. Jarrett et al. [31] interpreted the premelting behavior of *n*-alkanes as due to the change of molecular motion in the vicinity of the molecular ends. Ishikawa

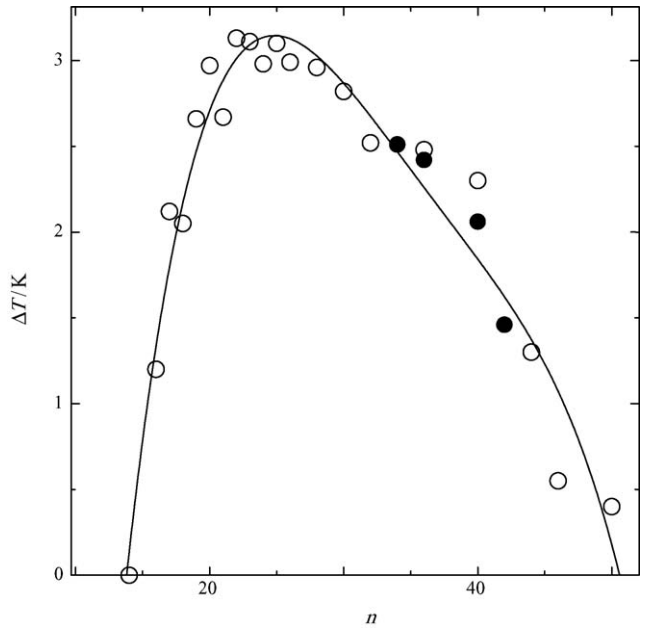

Fig. 6. The temperature difference ΔT between the melting point and the fusion temperature of the surface layer as a function of the carbon number n, where (◯) is the literature data [22] and (●) is present result.

et al. [41] observed the change of molecular motion of CH_3 and α-CH_2 between 313 and 343 K in $C_{32}H_{66}$. Although the mechanism of the new peaks detected in the M phase of all the samples is not so clear, it may be related to the disorder of the structure resulting from the active molecular motion in the vicinity of the molecular ends. The difference of the enthalpy changes of these peaks is considered to relate with the number of the CH_2 unit in the active molecular ends. The longer molecular chain is considered to make the enthalpy change larger as shown in Tables 1 and 2.

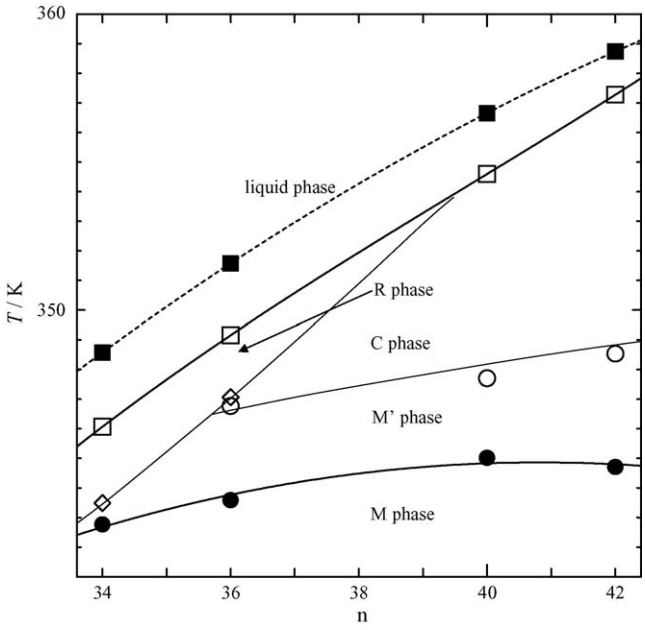

Fig. 7. The phase transitions in pure $C_{34}H_{70}$, $C_{36}H_{74}$, $C_{40}H_{82}$ and $C_{42}H_{86}$ obtained by present measurement in the heating run.

The thermal behavior of the samples in the heating run and cooling run was considerably different. The schematic drawing of the relative enthalpy versus temperature for each sample obtained by the present study is shown in Fig. 8, where the difference between the heating and the cooling run is observed more clearly. In Fig. 8 the transitions in the heating run are shown as the solid lines and those of cooling run are shown as the dotted lines. The Arabic numerals are corresponding to the peaks number of the DSC curves. The scales of vertical and horizontal axis are arbitrary in Fig. 8. The peak due to the transition from the R phase to the M phase of $C_{34}H_{70}$ separated into two peaks in the cooling run as seen peaks 3′ and 4′ in Fig. 2(b), showing the appearance of a new phase (C′ phase) as shown in Fig. 8(a). From Fig. 3(b) and Table 1, the intermediate form of $C_{36}H_{74}$ appeared in the cooling run (C′ phase) is considered different with that of heating run (C phase) as shown in Fig. 8(b). M′ phase appeared in the heating run in $C_{40}H_{82}$ and $C_{42}H_{86}$, but it was not observed in the cooling run as shown in Fig. 8(c). Since

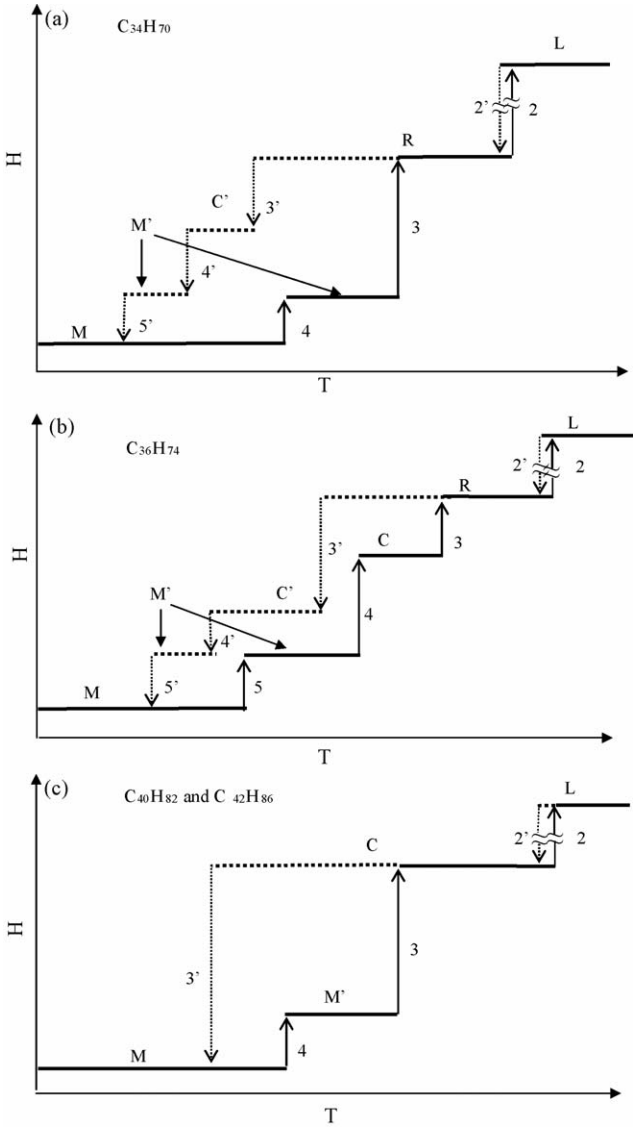

Fig. 8. Schematic drawing of the relative enthalpy vs. temperature for (a) $C_{34}H_{70}$, (b) $C_{36}H_{74}$, and (c) $C_{40}H_{82}$ and $C_{42}H_{86}$.

the mechanism of these transitions in the cooling run is not clear at present, further investigation is needed using X-ray and other analytical methods.

5. Conclusions

The new behaviors of the phase transitions in pure *n*-$C_{34}H_{70}$, *n*-$C_{36}H_{74}$, *n*-$C_{40}H_{82}$ and *n*-$C_{42}H_{86}$ have been found at the measuring conditions of slow heating and cooling rates using a high resolution and super-sensitive DSC.

(1) A new peak was detected in the low-temperature crystalline phase (M phase) of all the samples. It is considered to relate to the disorder of the structure resulting from the active molecular motion in the vicinity of the molecular ends.
(2) The surface freezing phenomenon was observed in all of the samples both in the heating and in the cooling run.
(3) The heat capacity of phase C is much larger than that of the liquid, considered to be related to the contribution of active vibrational motion.
(4) C′ phase was considered to exist in $C_{34}H_{70}$ in the cooling run.

References

[1] A. Müller, K. Lonsdale, Acta Crystallogr. 1 (1948) 129.
[2] H.M.M. Shearer, V. Vand, Acta Crystallogr. 9 (1956) 379.
[3] A.E. Smith, J. Chem. Phys. 21 (1953) 2229.
[4] K. Nozaki, N. Higashitani, T. Yamamoto, T. Hara, J. Chem. Phys. 103 (1995) 5762.
[5] W. Piesczek, G.R. Strobl, K. Malzahn, Acta Crystallogr. B30 (1974) 1278.
[6] I. Denicolo, J. Doucet, A.F. Craievich, J. Chem. Phys. 78 (1983) 1465.
[7] U. Domanska, D. Wyrzykowska, Thermochim. Acta 179 (1991) 265.
[8] H.L. Finke, M.E. Gross, G. Waddington, H.M. Huffman, J. Am. Chem. Soc. 76 (1954) 333.
[9] K. Nozaki, T. Yamamoto, T. Hara, M. Hikosaka, Jpn. J. Appl. Phys. 36 (1997) L146.
[10] T. Gorecki, S.P. Srivastava, G.B. Tiwari, Cz. Gorecki, A. Zurawska, Thermochim. Acta 345 (2000) 25.
[11] R. Kitamaru, F. Horii, M. Nakagawa, K. Takamizawa, Y. Urabe, Y. Ogawa, J. Mol. Struct. 355 (1995) 95.
[12] P.K. Sullivan, J.J. Weeks, J. Res. Natl. Bur. Stand. 74 (1970) 203.
[13] K. Takamizawa, Y. Ogawa, T. Oyama, Polym. J. 14 (1982) 441.
[14] H. Kraack, E.B. Sirota, M. Deutsch, J. Chem. Phys. 112 (2000) 6873.
[15] A. Briard, M. Bouroukba, D. Petitjean, N. Hubert, M. Dirand, J. Chem. Eng. Data 48 (2003) 497.
[16] M.G. Broadhurst, J. Res. Natl. Bur. Stand. Sect. A 66 (1962) 241.
[17] A. Müller, Proc. Roy. Soc. Lond. A 138 (1932) 514.
[18] J. Doucet, I. Denicolo, A. Graievich, J. Chem. Phys. 75 (1981) 1523.
[19] G. Ungar, J. Phys. Chem. 89 (1985) 1036.
[20] E.B. Sirota, H.E. King Jr., D.M. Singer, H.H. Shao, J. Chem. Phys. 98 (1993) 5809.
[21] E.B. Sirota, D.M. Singer, J. Chem. Phys. 101 (1994) 10873.
[22] B.M. Ocko, X.Z. Wu, E.B. Sirota, S.K. Sinha, O. Gang, M. Deutsch, Phys. Rev. E 55 (1997) 3164.
[23] X.Z. Wu, E.B. Sirota, S.K. Sinha, B.M. Ocko, M. Deutsch, Phys. Rev. Lett. 70 (1993) 958.
[24] H.Z. Li, T. Yamamoto, J. Chem. Phys. 114 (2001) 5774.
[25] T. Shimizu, T. Yamamoto, J. Chem. Phys. 113 (2000) 3351.
[26] M. Kawamata, T. Yamamoto, J. Phys. Soc. Jpn. 66 (1997) 2350.
[27] A. Wawkuschewski, H.J. Cantow, S.N. Magonov, Langmuir 9 (1993) 2778.
[28] S. Wang, K. Tozaki, H. Hayashi, S. Hosaka, H. Inaba, Thermochim. Acta 408 (2003) 31.
[29] B. Wunderich, Thermal Analysis, Academic press, New York, 1990.
[30] T. Hatakeyama, F.X. Quinn, Thermal Analysis: Fundamentals and Application to Polymer Science, Wiley, New York, 1994.
[31] W.L. Jarrett, L.J. Mathias, R.G. Alamo, L. Mandelkern, D.L. Dorset, Macromolecules 25 (1992) 3468.
[32] P. Barbillon, L. Schuffenecker, J. Dellacherie, D. Balesdent, M. Dirand, J. Chem. Phys. 88 (1991) 91.
[33] F.O. Cedeno, M.M. Prieto, A. Espina, J.R. Garcia, J. Therm. Anal. Calorim. 7 (2003) 775.
[34] S. Wang, K. Tozaki, H. Hayashi, H. Inaba, J. Therm. Anal. Calorim. 79 (2005) 605.
[35] K. Tozaki, H. Inaba, H. Hayashi, C. Quan, N. Nemoto, T. Kimura, Thermochim. Acta 397 (2003) 155.
[36] S. Hosaka, K. Tozaki, H. Hayashi, H. Inaba, Phys. B 337 (2003) 138.
[37] Y. Urabe, M. Saito, H. Fujiwara, N. Nemoto, Technol. Rep. Kyushu Univ. 72 (1994) 101.
[38] Y. Kim, H.L. Strauss, R.G. Snyder, J. Phys. Chem. 93 (1989) 7520.
[39] E.P. Gilbert, Phys. Chem. Chem. Phys. 1 (1991) 1517.
[40] K. Nakasone, K. Takamizawa, K. Shiokawa, Y. Urabe, Thermochim. Acta 233 (1994) 175.
[41] P. Ishikawa, H. Kurosu, I. Ando, J. Mol. Struct. 248 (1991) 361.